



Supplement of

Evolution of volatility and composition in sesquiterpene-mixed and α -pinene secondary organic aerosol particles during isothermal evaporation

Zijun Li et al.

Correspondence to: Angela Buchholz (angela.buchholz@uef.fi) and Annele Virtanen (annele.virtanen@uef.fi)

The copyright of individual parts of the supplement might differ from the article licence.

Supplement material

S1.1 Experimental approach for isothermal evaporation of secondary organic aerosol (SOA) particles

15 The experimental sequence consisted of SOA production, particle size selection, humidity-controlled SOA particle evaporation, and particle characterization. The schematic diagram of the experimental setup is shown in Figure S1, and the experimental conditions and results are summarized in Table S1.

S1.1.1 SOA Production

20 SOA was generated by oxidizing two different types of BVOCs in a 13 L oxidation flow reactor (OFR, Aerodyne Research Inc.) (Kang et al., 2007; Lambe et al., 2011)). Either α -pinene (Sigma-Aldrich, 98%) or a sesquiterpene mixture (Sigma-Aldrich, mixture of isomers) which consists of farnesenes and bisabolenes was used for generating SOA. A syringe pump system (Kari et al., 2018) was used to constantly inject liquid VOC precursors into 1.3 L min⁻¹ of heated N₂ flow. Before entering the OFR, the VOC-containing flow was mixed with a humidified flow of N₂ and O₃. To achieve the target RH, water vapor was introduced by passing 5.3 L min⁻¹ of N₂ through a Nafion humidifier (Model FC 100-80-6MSS, Perma Pure). O₃ was generated externally by passing 0.45 L min⁻¹ of O₂ via an ozone generator with a 185-nm UV lamp. Prior to mixing with O₃, the concentration of VOC was continuously monitored by a proton transfer reaction time-of-flight mass spectrometer (PTR-TOF 8000, Ionicon Analytik) using H₃O⁺ reagent ions. Eventually, 5.3 L min⁻¹ of total flow containing VOC (254 – 261 ppb) and O₃ (13.01 – 13.40 ppm) with RH of 41% - 44% was introduced into the OFR for photooxidation at controlled temperature (~ 25 °C), with 160 sec residence time inside the OFR.

30 Under the illumination of 254-nm lamps, O(¹D) was generated from the photolysis of O₃ and consecutively reacted with H₂O to produce OH radicals. We produced the α -pinene and the sesquiterpene mixture (SQTmix) SOA under comparable oxidation conditions. According to the OFR model (Peng et al., 2015; Peng et al., 2016) which accounts for the external OH activity, the OH exposure was between 0.9 and 2.6×10¹¹ molec cm⁻³, equivalent to 0.7 to 2 days of atmospheric aging. Before each SOA experiment, we conducted photochemical cleaning of the OFR overnight (~ 8 hr.) by flushing the OFR with purified air at the desired concentration of OH but without adding any VOC. After an overnight photochemical cleaning, the background particle number concentration was below 2000 # cm⁻³ (particle mass concentration < 0.1 µg m⁻³) and VOC concentration was below the instrument 35 limit of detection.

S1.1.2 Particle Size Selection

40 Following the SOA generation in the OFR, 2 L min⁻¹ of sample flow was passed through an ozone denuder coated with potassium iodide. Two parallel nanometer aerosol differential mobility analyzers (NanoDMA, model 3085, TSI) were then employed to select a narrow distribution of SOA particles with an electrical mobility diameter of 80 nm and simultaneously dilute the surround gas phase by two orders of magnitude, which initiates isothermal evaporation at the outlet of the NanoDMAs. To remove the majority of gas vapors, each NanoDMA was operated with an open loop sheath flow at a sample-to-sheath flow ratio of 1:8 or 1:10. To control the RH of the samples, we humidified/dried the sheath flow of the NanoDMAs by mixing a dry and a humidified air flow.

S1.1.3 Humidity-Controlled Particle Evaporation

45 After exiting the NanoDMAs, the monodisperse particle sample was fed (i) to bypass lines with varying lengths for short residence
time measurements of up to 3 min, (ii) to a 25 L stainless-steel residence time chambers (RTC) for intermediate measurements
with 10 min intervals for up to 40 min, or (iii) to a 100 L RTC for long measurements with 1 h intervals for up to 7.5 h. We initiated
the RTC experiments by filling the RTC with the monodisperse particle sample for 5 min (25 L RTC) or 20 min (100 L RTC).
After the particle filling, we immediately sealed the RTC. Periodically, the RTC was opened for sampling. At the same time,
50 purified air with the same RH was supplied to the RTC to compensate for the removed air volume to maintain constant pressure
and humidity, which resulted in a dilution factor below 1.2. For each SOA type, evaporation experiments were conducted under
one of three desired RH conditions (i.e., dry (< 7% RH), intermediate (40% RH), or high (80% RH)). Once each evaporation
experiment was completed, we flushed the NanoDMAs, bypass lines, and RTCs with purified air at the desired RH of the following
experiment for at least 12 h.

S1.1.4 Particle Characterization

55 The size changes of monodisperse SOA particles due to isothermal evaporation were measured by a scanning mobility particle
sizer (SMPS, model 3080, TSI). Since we only rely on the particle size to evaluate the extent of particle evaporation, any decrease
in the particle number or mass concentration (due to, e.g., wall losses or dilution) only limits the number of times for particle
sampling from the RTC. The selected particle size was calibrated against dry ammonium sulfate particles. The volume fraction
remaining (VFR) was calculated as the cubic ratio of the particle size ($D_{p,t}$) measured after time t of evaporation and the selected
60 size ($D_{p,0}$) at the start of evaporation as follows:

$$VFR = \left(\frac{D_{p,t}}{D_{p,0}}\right)^3 \quad (\text{S1, Eq. 1 in main text})$$

The elemental composition of the particle sample was determined using a high-resolution time-of-flight aerosol mass spectrometer
(HR-ToF-AMS, Aerodyne Research Inc.) and was analyzed using the TOF-AMS toolkits (SQUIRREL 1.59C and PIKA 1.19C).
We determined the oxidation state ($\text{OSc} = 2 \times \text{O}:\text{C} - \text{H}:\text{C}$) of monodisperse particle samples exiting the NanoDMAs with the
65 improved ambient parameterizations (Canagaratna et al., 2015). As the particle concentration after the RTC evaporation was too
low for reliable elemental composition measurements, we only present the compositional data from the bypass tubing
measurements which exhibited the least amount of isothermal evaporation.

The thermal desorption behavior and chemical composition of particle samples were characterized using a custom-built Filter Inlet
for Gases and AEROsols (FIGAERO) (Ylisirniö et al., 2021) in combination with a chemical ionization mass spectrometer (CIMS,
70 Aerodyne Research Inc.) using iodide as reagent ion (Lopez-Hilfiker et al., 2014). The mass resolution CIMS was ranging from
4000 to 5000 and the pressure of the ion molecule reaction (IMR) chamber was constantly maintained at 100 mbar. Each particle
sample after size selection (i.e., fresh samples) or isothermal evaporation in the RTC (i.e., RTC samples) was collected for analysis
on a PTFE filter (2 μm pore, Zefluor, Pall Corp.) for 30 min in the FIGAERO. After sample collection, the collected particles were
desorbed with a N_2 flow of which the temperature was linearly increased from 25 $^\circ\text{C}$ to ~ 190 $^\circ\text{C}$ in 20 min (desorption period) and
75 maintained at above 190 $^\circ\text{C}$ for additional 15 min (soak period). The relationship between the temperature of maximum desorption
signal (T_{max}) of a single compound and its saturation vapor concentration (C^*) was calibrated by measuring polyethylene glycol

(PEG, PEG 4 - 8) particles with known vapor pressures (p_{sat}) (Ylissirniö et al., 2021). The $T_{max} - p_{sat}$ relationship used in the study can be expressed as $\ln(p_{sat}) = -0.21 \times T_{max} - 0.62$.

80 The analysis of the raw FIGAERO-CIMS data was performed using Tofware (version 3.2, TOFWERK AG). Prior to fitting the high-resolution mass spectra data, the data were averaged over 10 sec of measurement time and a baseline correction was applied. The filter blank samples were analyzed in the same manner as the particle samples. To identify instrument background and contamination from the surrounding gas, we performed two types of blank measurements: (i) Measurements of the clean FIGAERO filter without collecting particles for characterizing the overall instrument background. (ii) Measurements of filter sampled after size selection for 30 min but with the NanoDMAs voltage set to 0V for characterizing the background due to adsorption of gas-
85 phase compounds during the time of normal sample collection.

In the absence of a reliable transmission and sensitivity calibration for the relevant compounds detected with FIGAERO-CIMS, we assume uniform sensitivity and transmission for all ions. We conducted SMPS measurements prior to the FIGAERO-CIMS sample collection. Accounting for the amount of particulate water, changes in the VFR and organic density, we derived the theoretical collected mass on the filter from the sampled volume for the fresh stages. For the RTC stages, particles in the 100-L
90 RTC were assumed to be 100% collected on the FIGAERO filter to provide an upper limit of the collected amount. As shown in Figure S2, the collected mass is almost linearly correlated with the total signal of sample factor between conditions, which validates the normalization methods used in this study. The collected mass seems to be overestimated for the two high-RH RTC samples. These experiments proved to be the most challenging to collect sufficient material on the filter. However, we could not rule out if there were increased particle losses in the transfer from the RTC to the filter or if other issues led to the overestimation from the
95 SMPS measurements.

S1.2 Analysis of FIGAERO-CIMS data using positive matrix factorization (PMF)

S1.2.1 General method and selection of error scheme

The PMF model expresses the measured mass spectra matrix X by a combination of a number, p , of constant factors with varying concentrations with time (Paatero and Tapper, 1994; Ulbrich et al., 2009):

$$100 \quad X = GF + E \quad (S2)$$

X is a $m \times n$ matrix containing the measured mass spectra, with m rows of mass spectra averaged over 10 sec of measurement time and n columns containing the time series of one specific ion. G is a $m \times p$ matrix containing the factor time series as columns. The rows of the $p \times n$ matrix F contain the factor mass spectra. Then the $m \times n$ matrix E contains the residuals between the measured data and the fitted values. To account for uncertainties in the measurement data, the PMF model weights the data points with their measurement error (S_{ij}). Values for G and F are constrained to be positive and iteratively found by minimizing the quantity (Q)
105 with a least square algorithm (Paatero and Tapper, 1994):

$$Q = \sum_{j=1}^m \sum_{i=1}^n \left(\frac{E_{ij}}{S_{ij}} \right)^2 \quad (S3)$$

S_{ij} is the error (uncertainty) of each measurement data point. In an ideal case, the Q value of the model should approach the expected Q value ($Q_{exp} \approx n \cdot m$) which is equal to the degree of freedom of the model solution.

110 The chosen measurement error values have a direct impact on the performance of the PMF algorithm. We tested the two schemes suggested in Buchholz et al. (2020) with and without downweighing of low intensity signals. Assuming a Poisson-like distribution for the counting statistics of the mass spectrometer, the error values $S_{PL,ij}$ were calculated with

$$S_{PL,ij} = a \cdot (X_{ij})^c + b \quad (S4)$$

where X_{ij} is the signal intensity of the ion i at temperature/time j . a , b , and c are empirical parameters derived from the data set as described in (Buchholz et al., 2020). Here, their values are: $a = 0.62$, $b = 0.076$, and $c = 0.39$. For the constant error scheme (CN), which has a constant error value for one ion during one thermogram, the final 200 sec of the soak period were used to determine the noise value for each ion. The ion thermograms were smoothed with a Savitzky-Golay filter. The residual between these smoothed ion thermograms and the measured ion thermograms were calculated. The standard deviation of these residual for each ion was then set as the noise of this ion and used as its CN error value. For both error schemes, a minimum error value was applied. 120 This was equal to the median of the CN error values (MinErr, 0.48 and 0.50 for the α -pinene and SQTmix cases, respectively).

As both error schemes are not necessarily representing the “true” measurement error, the criteria $Q/Q_{exp} \rightarrow 1$ may not be satisfied. Apart from the overall change in Q/Q_{exp} , we also include the relative residual, how well peak shapes of ions are reproduced, and the overall interpretability of the factors as comprehensive measures of the quality of the PMF solution.

With the PL error scheme, the performance of the PMF algorithm was generally not satisfactory even with 12 factors. The PMF model underestimated the measured signals especially for the region around the T_{max} values of strong ions. Downweighing weak ions (signal to noise ratio < 2) did not improve this behavior. The unexplained variance could not be reduced below 10%. On the other hand, the CN error scheme yielded smaller overall residual values and unexplained variance values of $< 1\%$. The residuals were distributed more evenly around 0 for each ion (i.e., no bias towards underestimation). For the CN error scheme, downweighing weak ions did not change the overall interpretation of the PMF factors. We thus decided to present the solution with the CN error and no downweighing in the manuscript. 130

S1.2.2 Selection of the optimal PMF solution

The most subjective part of PMF analysis is the selection of the optimal solution, i.e., the number of factors. We carefully inspected solutions with up to 10 factors for the α -pinene samples or 12 factors for the SQTmix ones with multiple rotations. According to our evaluation criteria for the quality of the PMF solution, the eight-factor solution at $f_{peak} = 0$ was selected for the α -pinene SOA data set. In the same way, the ten-factor solution at $f_{peak} = -0.5$ was chosen for the SQTmix SOA data set, which yielded the most interpretable results. The PMF results are presented in Figure S3 and S4. Note that compared to the α -pinene case, the two additional factors were necessary to capture the more complex background in the SQTmix case. I.e., for the SQTmix SOA data, the composition and signal strength of the background varied between experiment days, most likely due to some additional contamination of the setup caused by the necessary maintenance. 135

Figure S5 shows the Q/Q_{exp} vs number of factor curve for both data sets. The unscaled residuals, relative residuals, and scaled residuals of the 6-8 factor solution (8-10 factors, respectively) are depicted in Figure S6 for both data sets. Already with six factors for the α -pinene SOA particles (or eight factors for the SQTmix SOA particles, respectively), the residuals were in an acceptable range (relative residuals $< 5\%$ for most of the data set) and the change in Q/Q_{exp} was only gradual. However, increasing from six to seven factors for the α -pinene SOA particles or eight to nine for the SQTmix SOA particles improved the reconstruction of many ion peak shapes, especially for the high RH samples. This suggests that the additional factor enhanced the separation of the 145

effect of isothermal evaporation from aqueous phase processes. With one more factor (eight and ten factors for the α -pinene and SQTmix SOA particles), the aqueous phase processes became even more visible in the factors. Thus, these solutions were selected for the detailed interpretation presented in the main manuscript. Increasing the number of factors further, either introduced more background factors or clearly splitted one of the existing sample factors into two. The overall interpretation of the PMF solution would not be changed.

S1.2.3 Discussion on changes in characteristic T_{desorp} and thermogram shapes of PMF factors

The PMF algorithm identifies correlations between variables in a data set. The interpretation of this mathematical concept is that PMF finds the parts of the signals (ions) that correlate with each other. The reason for that correlation can be a common source or formation process. For FIGAERO thermogram data, it can be similar desorption behavior (i.e., similar volatility). If this interpretation is valid, how can the shifts in characteristic T_{desorp} be explained for AF1 and SF1? And why does the shape of some factor thermograms change so dramatically between the dry and wet case (e.g., AF3 and SF3)? In this section, we will address the shift of the characteristic T_{desorp} at first and then provide some additional thoughts about the possible reasons for the thermogram shape change.

We will use a simplified artificial data set to illustrate the performance of the PMF algorithm. This data set contains 4 “ions” that would be detected by FIGAERO-CIMS. Each ion is constructed using compounds with distinct volatility behavior characterized by their T_{max} and remaining fraction after evaporation. The ions #1 - #3 contain only one compound each (A1, B1, C1, respectively). Ion #4 contains 3 compounds (A2, B2 and C2). The same letter in the compound label means that the compounds exhibit the same volatility. E.g., A1 and A2 both have a T_{max} of 50 °C and show an isothermal evaporation to 0.1 of their starting value.

The thermograms of the individual compounds were constructed as gaussian curves with some random noise.

$$I(T) = 100 * \exp\left(-\left(\frac{T-T_{\text{max}}}{5}\right)^2\right) + \textit{noise} \quad (\text{S5})$$

with $I(T)$ intensity of the single compound thermogram, T_{max} peak position of the thermogram and *noise* random noise term.

The ions are formed by using multiples of these compound thermograms ($I_a(T)$, $I_b(T)$, $I_c(T)$) or combinations of them (for ion #4), as summarized in Table S2. Two SOA samples were created: Sample #1 which mimics the fresh case with no evaporation and sample #2 in which the volatile compounds (A1, A2, B1, and B2) have evaporated according to their volatility. The ion thermograms for these samples are shown in Figure S7. Note that the ratios between A2 and B2 are different for the two samples. PMF finds a fairly good solution with 2 factors (see Figure S8 and Table S3): F2 containing C1&2 is identical for sample #1 and #2 as it should be. F1 contains compounds A1&2 and B1&2. The T_{max} value of F1 are 52 and 53 °C for the two samples and the shape of the factor thermogram changes. As the ratio between A and B changes between two samples (i.e., A1&2 are more efficiently removed by isothermal evaporation than B1&2), the smallest residuals are achieved by shifting the thermogram of F1 towards the T_{max} value of B1&2. The PMF reconstruction will not be “perfect” for either sample since neither A1&2 nor B1&2 are captured completely. However, a 2-factor solution is sufficient for interpreting the overall evaporation behavior. We can easily see that F1 is removed with isothermal evaporation and F2 remains (Figure S8a). In a 3-factor solution (see Figure S8b and Table S3), A1&2 and B1&2 are separated into two factors F3 and F1 and no change in the thermogram shapes are observed between the samples. For the interpretation, we can state that F3 is a bit more volatile than F1 and both are systematically removed by isothermal evaporation.

In a real SOA particle sample, hundreds of compounds covering a range of volatilities are present. One FIGAERO-CIMS ion with a single elemental composition can contain multiple isomers and/or fragments from multiple different parent compounds. These real compounds within one elemental composition may have different desorption behavior (like the A, B, and C compounds in the example above). PMF groups the compounds with the most similar desorption behavior into a few factors with fixed ratios between the ion contributions. The result is always a compromise between finding as few factors as possible and reconstructing the majority of the ion thermograms correctly. For the case of AF1 and SF1, PMF finds the compounds/signals which are most similar (but not identical) in their evaporation behavior. The desorption behavior of the compounds in these factors span over a narrow T_{\max} -range which we characterize with the characteristic T_{desorp} (e.g., Fig 5a and 6a). During isothermal evaporation, the most volatile fraction of the factor evaporates a little bit more than the rest. Ideally, we would allow adjustments in the factor mass spectrum to account for these changes. However, PMF is not able to do that by design. Instead, it finds a nearly optimal compromise by increasing the characteristic T_{desorp} of the factor to minimize the residuals for all ions present in the factor. Figure S9 shows the behavior of 3 different ions which have a strong contribution to AF1 (factor thermogram shown in red (dry) and blue (high RH)). In the dry and fresh sample (red lines), the single ion thermograms are well reconstructed by PMF (i.e., very small difference between dash vs solid red lines). In the high RH and fresh sample (blue lines), one ion is still reconstructed well (c), one shows an underestimation around $T_{\text{desorp}} 100\text{ }^{\circ}\text{C}$ (b), and one exhibits an overestimation in that T_{desorp} range (a). This difference in residuals indicates that these 3 ions are experiencing different changes under high RH conditions. I.e., their “contribution” to the factor mass spectrum has changed somewhat. We carefully inspected the residuals for the reconstructed ion thermograms and found that for each factor with a significant change in thermogram shape, there were some ions which changed their “goodness of reconstruction” in the relevant T_{desorp} range.

One would assume that this “issue” could be fixed in the same way as for the simple artificial sample above by adding one more factor. We tested the α -pinene data with up to 12 factors and the SQTmix data with 13 factors (i.e., 4 more than in the presented solution). We did not see that the introduction of a factor would separate this slightly different desorption behavior. A splitting into AF1a and AF1b may happen eventually after the occurrence of severe factor splitting and the introduction of multiple “noise” factors. The primary aim of a PMF analysis is to reduce the number of variables for the interpretation step and to identify underlying trends in the data. The behavior of AF1 was interpreted as a systematic removal of compounds mostly affected by isothermal evaporation. A further splitting of AF1 does not provide any additional insight into the overall evaporation behavior of the SOA samples.

For the second type of change in factor thermogram shape exhibited e.g., by AF3 and SF3, it is necessary to consider aqueous phase processes. The volatility of the factors exhibiting this type of change is in the LVOC or ELVOC range (e.g., AF3). No significant isothermal evaporation is expected for compounds within this range. For AF3, there was a higher contribution of SVOC compounds in the high RH and fresh case which cannot be explained with any isothermal evaporation pathway. With the available data, we cannot give a definite answer to why these strong changes occur. But we can try to provide a plausible explanation.

The reason for the observed factor thermogram behavior may be connected to the fact that the ions detected in FIGAERO-CIMS are not always the same as the molecules in the particle. One possibility can be thermal-induced changes like decarboxylation or dehydration. Another possible option is the thermal decomposition of true dimers (or oligomers) into the monomer units. Assume there are the compounds A, B, C with similar desorption behavior in the sample under dry conditions. They are detected as the ions with the corresponding sum formulas A, B, C. If some of these compounds are “activated” in an aqueous phase to form dimers (e.g., via (hemi-)acetal bonds), there would be the compounds A-B, A-A, A-C, etc. in the sample under high RH conditions.

Presumably, the volatility of such dimers is lower than that of the monomer units. But the coupling bond may not be very strong. Very likely, before these compounds can thermally desorb from the FIGAERO filter, the bond is already broken which leads to the release of the original monomers. The detected ions in FIGAERO-CIMS would again show up as A, B, C with (almost) identical ratios as in the dry case. But T_{desorp} would have shifted to higher values as now we observe thermal decomposition of the dimers instead of direct desorption of the monomers. One can further speculate that with increasing reaction time (i.e., the time in the RTC), the fraction of (low-volatility) oligomers increases which increases the apparent characteristic T_{desorp} of the factor even further.

As the shifts are mostly observed comparing the dry to high RH conditions, the presence of water must play an important role. It could be that the high viscosity in the dry particles also limits the formation processes of such oligomers. The reaction partners have to meet each other which may be very slow in a (semi-)solid phase. But water could also be involved directly in the formation processes. Many of the suggested coupling reactions (e.g., esterification), are catalyzed by available H^+ or OH^- in a liquid phase. Similar ideas of reversible oligomer formation have been explored in model calculations (Schobesberger et al., 2018) and were suggested by D'Ambro et al. (2018), Zaveri et al. (2020) and Pospisilova et al. (2021) to explain their observations. Especially for small highly oxygenated ions (e.g., $\text{C}_2\text{H}_2\text{O}_3$), the main source seems to be decomposition of different parent compounds at different T_{desorp} values.

We want to highlight that even with these limitations in separating certain detailed trends in volatility, PMF analysis of FIGAERO-CIMS thermogram data is still a very powerful tool for discovering the links of particle composition and volatility. No a priori knowledge of physical or chemical parameters like the desorption enthalpy as well as the pathways of oligomer formation and decomposition are needed. No predefined volatility classes are assumed. Together with a thorough $T_{\text{max}}\text{-}p_{\text{sat}}$ calibration the results from a PMF analysis can instead help to constrain these parameters in process model calculations (Tikkanen et al., 2020).

- Buchholz, A., Ylisirniö, A., Huang, W., Mohr, C., Canagaratna, M., Worsnop, D. R., Schobesberger, S., and Virtanen, A.: Deconvolution of FIGAERO–CIMS thermal desorption profiles using positive matrix factorisation to identify chemical and physical processes during particle evaporation, *Atmos. Chem. Phys.*, 20, 7693-7716, 2020.
- 245 Canagaratna, M. R., Jimenez, J. L., Kroll, J. H., Chen, Q., Kessler, S. H., Massoli, P., Hildebrandt Ruiz, L., Fortner, E., Williams, L. R., Wilson, K. R., Surratt, J. D., Donahue, N. M., Jayne, J. T., and Worsnop, D. R.: Elemental ratio measurements of organic compounds using aerosol mass spectrometry: Characterization, improved calibration, and implications, *Atmos. Chem. Phys.*, 15, 253-272, 2015.
- 250 D'Ambro, E. L., Schobesberger, S., Zaveri, R. A., Shilling, J. E., Lee, B. H., Lopez-Hilfiker, F. D., Mohr, C., and Thornton, J. A.: Isothermal evaporation of α -pinene ozonolysis SOA: Volatility, phase state, and oligomeric composition, *ACS Earth and Space Chemistry*, 2, 1058-1067, 2018.
- Kang, E., Root, M. J., Toohey, D. W., and Brune, W. H.: Introducing the concept of potential aerosol mass (PAM), *Atmos. Chem. Phys.*, 7, 5727-5744, 2007.
- Kari, E., Miettinen, P., Yli-Pirilä, P., Virtanen, A., and Faiola, C. L.: PTR-ToF-MS product ion distributions and humidity-dependence of biogenic volatile organic compounds, *Int. J. Mass spectrom.*, 430, 87-97, 2018.
- 255 Lambe, A. T., Onasch, T. B., Massoli, P., Croasdale, D. R., Wright, J. P., Ahern, A. T., Williams, L. R., Worsnop, D. R., Brune, W. H., and Davidovits, P.: Laboratory studies of the chemical composition and cloud condensation nuclei (CCN) activity of secondary organic aerosol (SOA) and oxidized primary organic aerosol (OPOA), *Atmos. Chem. Phys.*, 11, 8913-8928, 2011.
- Lopez-Hilfiker, F. D., Mohr, C., Ehn, M., Rubach, F., Kleist, E., Wildt, J., Mentel, T. F., Lutz, A., Hallquist, M., 260 Worsnop, D., and Thornton, J. A.: A novel method for online analysis of gas and particle composition: Description and evaluation of a filter inlet for gases and aerosols (FIGAERO), *Atmos. Meas. Tech.*, 7, 983-1001, 2014.
- Paatero, P. and Tapper, U.: Positive matrix factorization: A non-negative factor model with optimal utilization of error estimates of data values, *Environmetrics*, 5, 111-126, 1994.
- Peng, Z., Day, D. A., Ortega, A. M., Palm, B. B., Hu, W. W., Stark, H., Li, R., Tsigaridis, K., Brune, W. H., and 265 Jimenez, J. L.: Non-OH chemistry in oxidation flow reactors for the study of atmospheric chemistry systematically examined by modeling, *Atmos. Chem. Phys.*, 16, 4283-4305, 2016.
- Peng, Z., Day, D. A., Stark, H., Li, R., Lee-Taylor, J., Palm, B. B., Brune, W. H., and Jimenez, J. L.: Hox radical chemistry in oxidation flow reactors with low-pressure mercury lamps systematically examined by modeling, *Atmos. Meas. Tech.*, 8, 4863-4890, 2015.
- 270 Pospisilova, V., Bell, D. M., Lamkaddam, H., Bertrand, A., Wang, L., Bhattu, D., Zhou, X., Dommen, J., Prevot, A. S., and Baltensperger, U.: Photodegradation of α -pinene secondary organic aerosol dominated by moderately oxidized molecules, *Environ. Sci. Technol.*, 55, 6936-6943, 2021.
- Schobesberger, S., D'Ambro, E. L., Lopez-Hilfiker, F. D., Mohr, C., and Thornton, J. A.: A model framework to retrieve thermodynamic and kinetic properties of organic aerosol from composition-resolved thermal desorption 275 measurements, *Atmos. Chem. Phys.*, 18, 14757-14785, 2018.
- Tikkanen, O.-P., Buchholz, A., Ylisirniö, A., Schobesberger, S., Virtanen, A., and Yli-Juuti, T.: Comparing secondary organic aerosol (SOA) volatility distributions derived from isothermal SOA particle evaporation data and FIGAERO–CIMS measurements, *Atmos. Chem. Phys.*, 20, 10441-10458, 2020.
- 280 Ulbrich, I. M., Canagaratna, M. R., Zhang, Q., Worsnop, D. R., and Jimenez, J. L.: Interpretation of organic components from positive matrix factorization of aerosol mass spectrometric data, *Atmos. Chem. Phys.*, 9, 2891-2918, 2009.
- Ylisirniö, A., Barreira, L. M. F., Pullinen, I., Buchholz, A., Jayne, J., Krechmer, J. E., Worsnop, D. R., Virtanen, A., and Schobesberger, S.: On the calibration of FIGAERO-tof-CIMS: Importance and impact of calibrant delivery for the particle-phase calibration, *Atmos. Meas. Tech.*, 14, 355-367, 2021.
- 285 Zaveri, R. A., Shilling, J. E., Zelenyuk, A., Zawadowicz, M. A., Suski, K., China, S., Bell, D. M., Veghte, D., and Laskin, A.: Particle-phase diffusion modulates partitioning of semivolatile organic compounds to aged secondary organic aerosol, *Environ. Sci. Technol.*, 54, 2595-2605, 2020.

Table S1. Experimental conditions and results for biogenic SOA generated from the OFR

	α -pinene	sesquiterpene mixture
abbreviation	α -pinene	SQTmix
[VOC] _{OFR} (ppb) ^a	254 ± 11	261 ± 5
[O ₃] _{OFR} (ppm) ^b	9.76 ± 0.31	9.55 ± 0.37
T _{OFR} (°C)	24.6 ± 0.9	25.50 ± 0.81
RH _{OFR} (%)	44.4 ± 2.3	40.86 ± 0.99
residence time (s)	160	161
effective OH exposure (10 ¹¹ molec cm ⁻³) ^c	2.6 ± 0.3	0.9 ± 0.1
oxygen-to-carbon (O:C) ^d	0.77 ± 0.03	0.95 ± 0.06
oxidation state (OSc) ^d	0.05 ± 0.04	0.50 ± 0.17

290 ^a Mixing ratio of VOC was corrected with the dilution of O₃-contained flow but without the loss due to pure ozonolysis at the inlet.

^b O₃ was measured at the OFR outlet after 254-nm UV lamps were switched on but without the addition of VOC precursors.

^c OH exposure was calculated with the OFR model (Peng et al., 2015; Peng et al., 2016) by taking the external OH reactivity into account.

295 ^d The values of the oxygen-to-carbon ratio (O:C) and the oxidation state (OSc) were derived from the HR-ToF-AMS measurement data of monodisperse SOA particles which represents the particle population used for isothermal evaporation measurements.

Table S2. Summary of ions in the artificial data set

	Compounds	$T_{\max} / ^\circ\text{C}$	Remaining Fraction	Thermogram – Sample #1	Thermogram – Sample #2
ion #1	A1	50	0.1	$0.75 \times I_a(T)$	$0.075 \times I_a(T)$
ion #2	B1	55	0.5	$0.75 \times I_b(T)$	$0.375 \times I_b(T)$
ion #3	C1	70	1.0	$0.5 \times I_c(T)$	$0.50 \times I_c(T)$
ion #4	A2, B2, C2	multi-modal	complex	$1.0 \times I_a(T) + 1.0 \times I_b(T) + 1.0 \times I_c(T)$	$0.1 \times I_a(T) + 0.5 \times I_b(T) + 1.0 \times I_c(T)$

Table S3. Compound distributions in PMF factor solutions in the artificial data set

Solution	F1	F2	F3
2 – factor solution	A1, A2, B1, B2	C1, C2	N/A
3 – factor solution	B1, B2	C1, C2	A1, A2

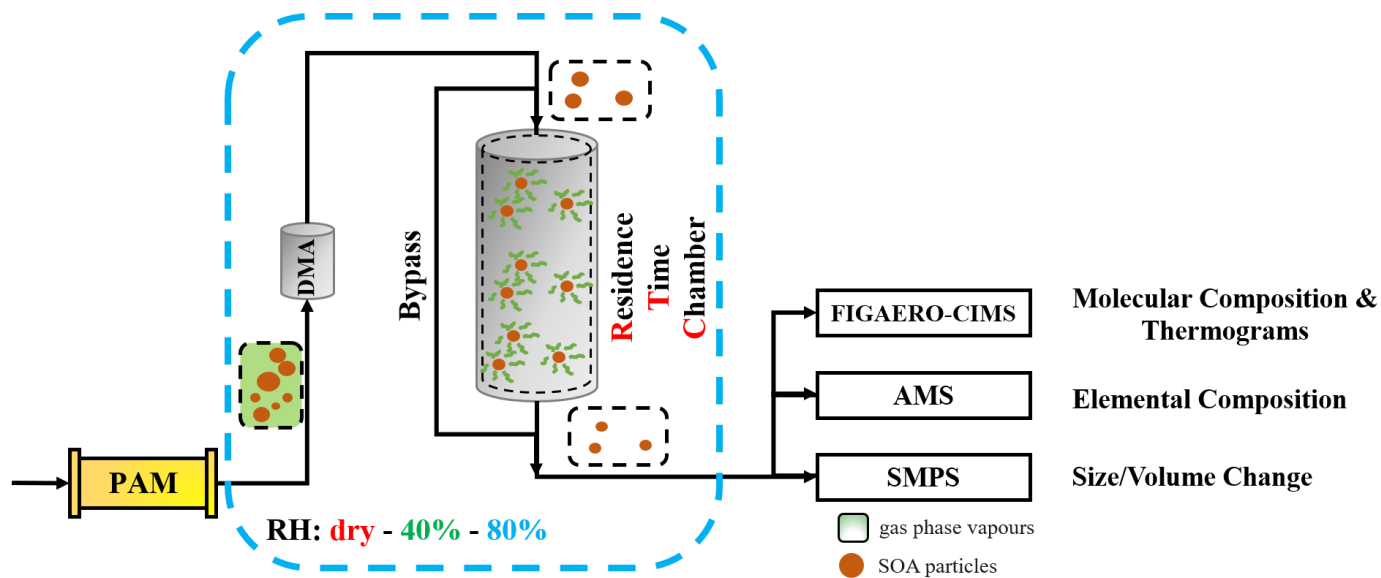
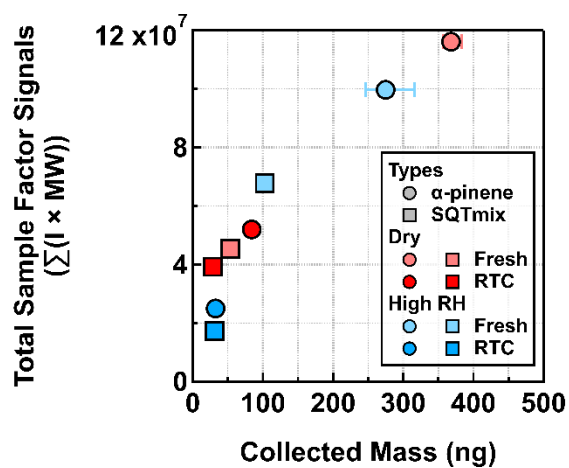


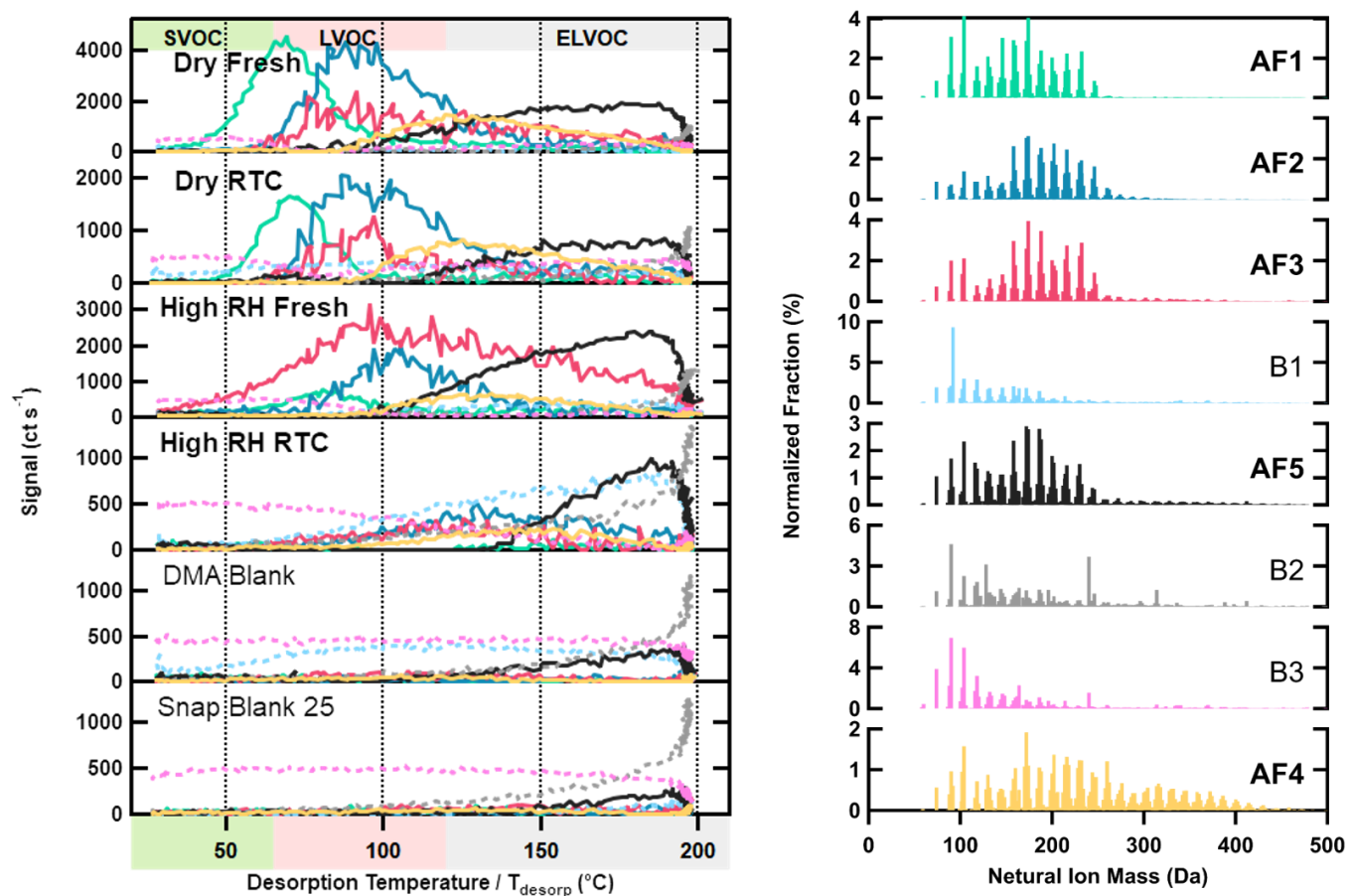
Figure S1. Experimental setup for evaporation experiments of α -pinene and sesquiterpene-mixed (SQTmix) SOA particles. Parts in the blue-dashed area were regulated with active humidity control.



305

Figure S2. Association between total sample signals of FIGAERO-CIMS and collected mass derived from SMPS measurements. The total sample signal is calculated as the product of signal intensity (I) and molecular weight (MW). This allows for a convenient cross-instrument comparison between FIGAERO-CIMS and SMPS. Unity sensitivity was applied for FIGAERO-CIMS data, while 100% filter collection efficiency was applied for deriving the collected mass from SMPS data. The error bar in the x axis indicates the range of collected mass.

310



315 **Figure S3.** Sample (solid lines) and background (dashed lines) factors from an eight-factor PMF solution for α -pinene SOA particles. Factor thermograms are shown with color bands indicating volatility categorization on the left panel, while normalized factor mass spectrums are presented on the right panel. The color code is identical for both panels.

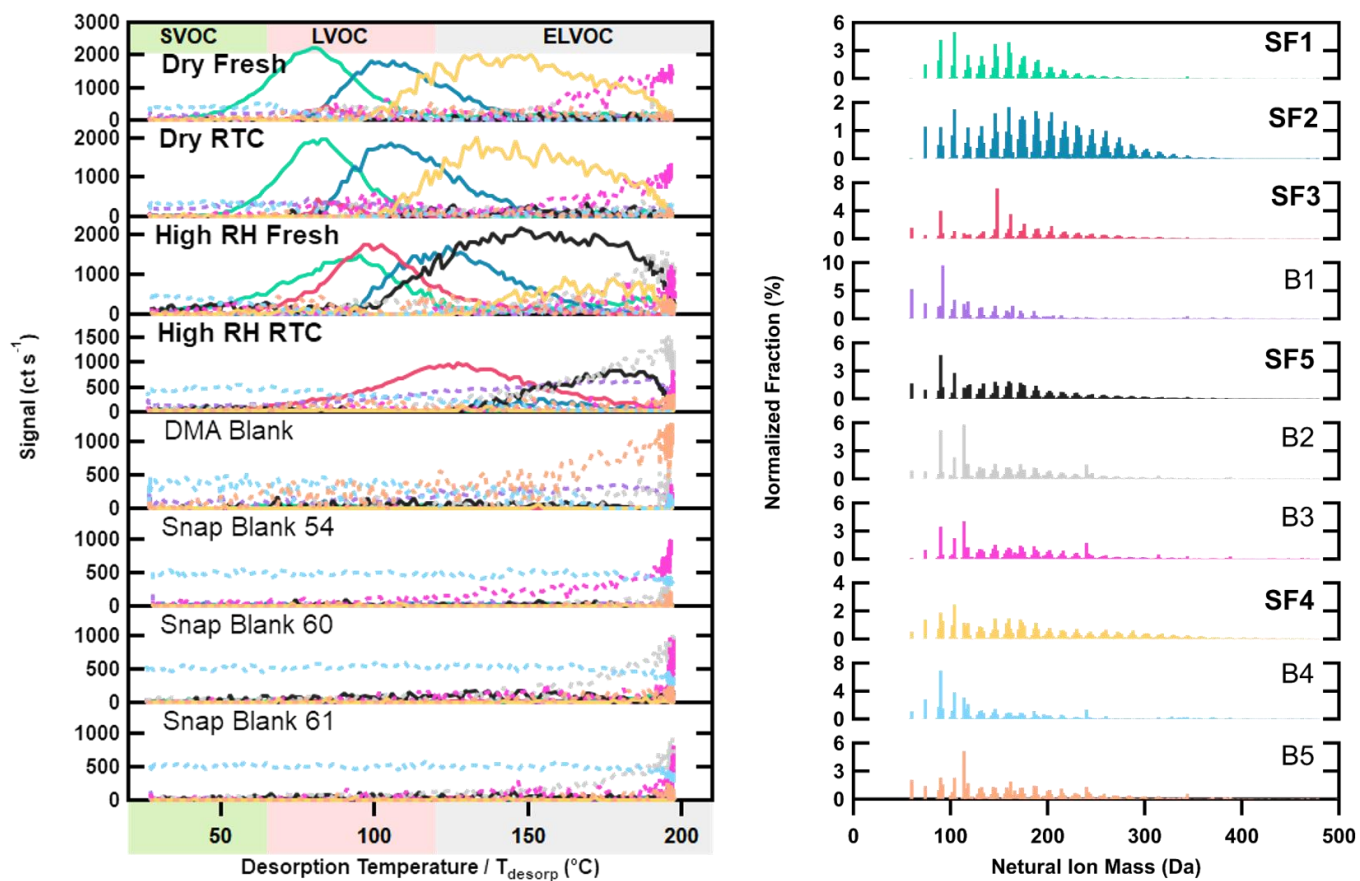


Figure S4. Sample (solid lines) and background (dashed lines) factors from a ten-factor PMF solution for SQTmix SOA particles. Factor thermograms are shown with color bands indicating volatility categorization on the left panel, while normalized factor mass spectrums are presented on the right panel. The color code is identical for both panels.

320

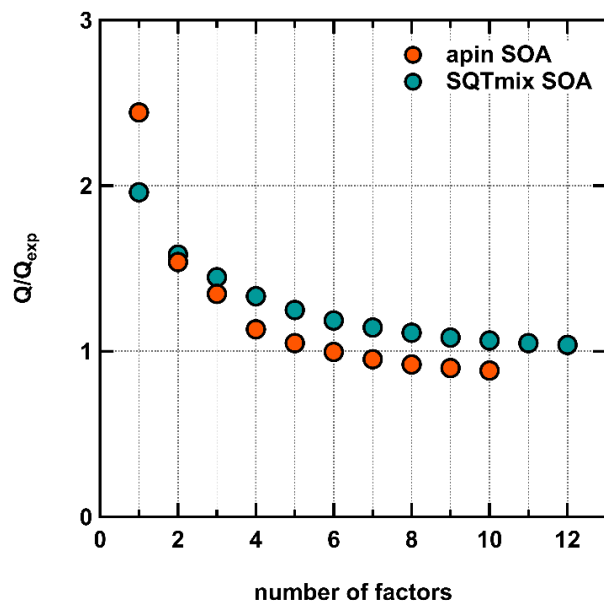
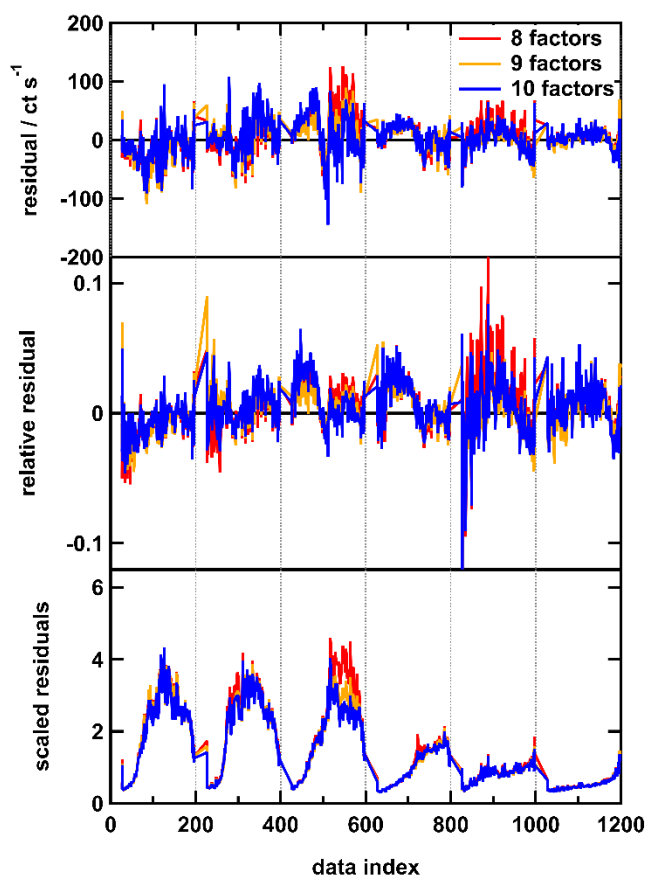
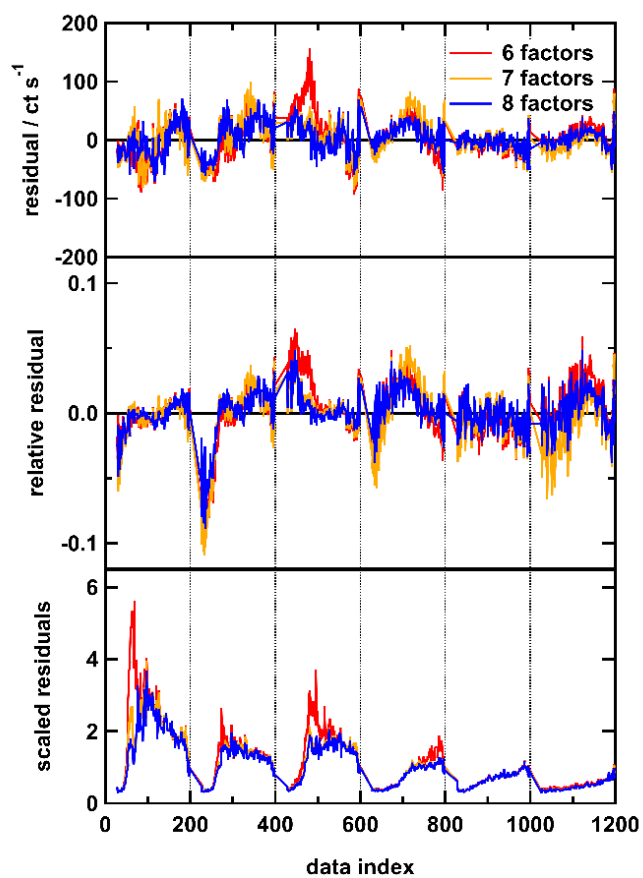


Figure S5. Q/Q_{exp} values for PMF solutions for α -pinene (orange) and SQTmix (turquoise) SOA data sets.



325

Figure S6. “Time” series of residuals, relative residuals, and scaled residuals for the 6 – 8 factor solutions for the α -pinene SOA data set (left) and the 8 – 10 factor solutions of the SQTmix SOA data set (right). The four samples and two blanks are plotted vs a data index which is $T_{\text{desorp}} + (i \cdot 200 \text{ } ^\circ\text{C})$. Vertical dashed lines indicate the start of the next sample. The order is: fresh, dry (0-200); RTC, dry (200-400); fresh, high RH (400-600); RTC, high RH (600-800); DMA blank (800-1000); snap blank (1000-1200).

330

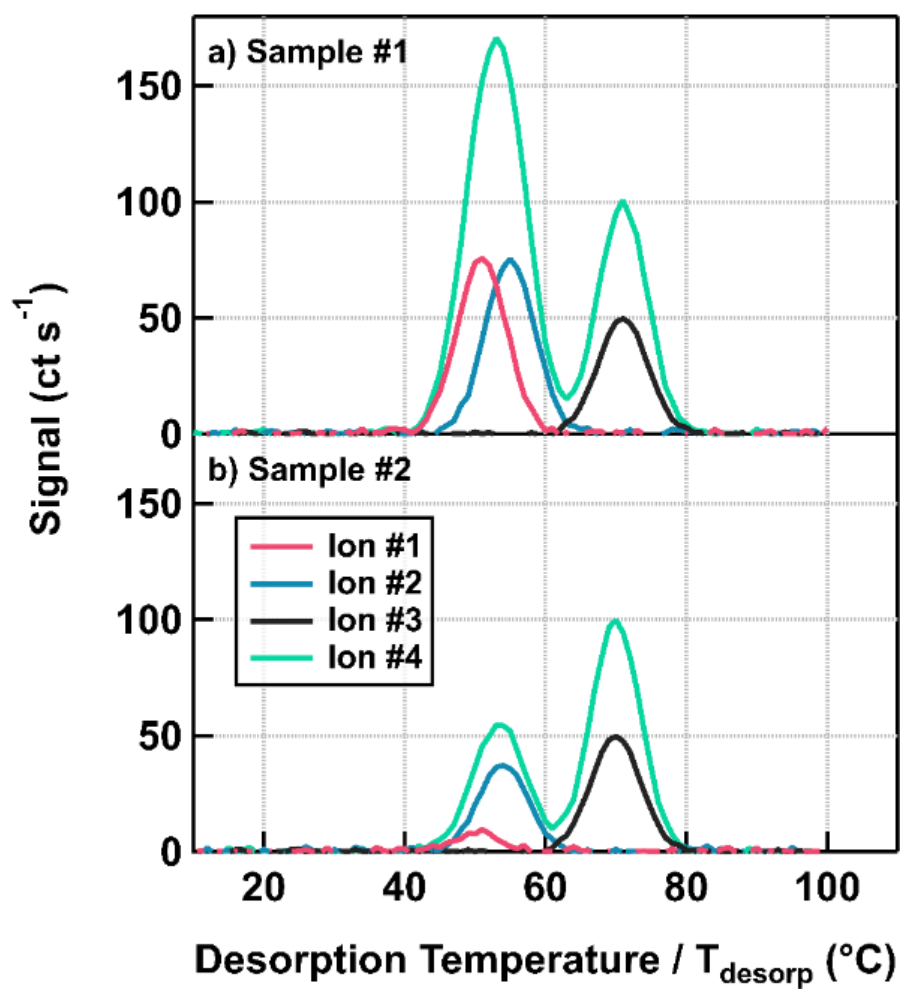
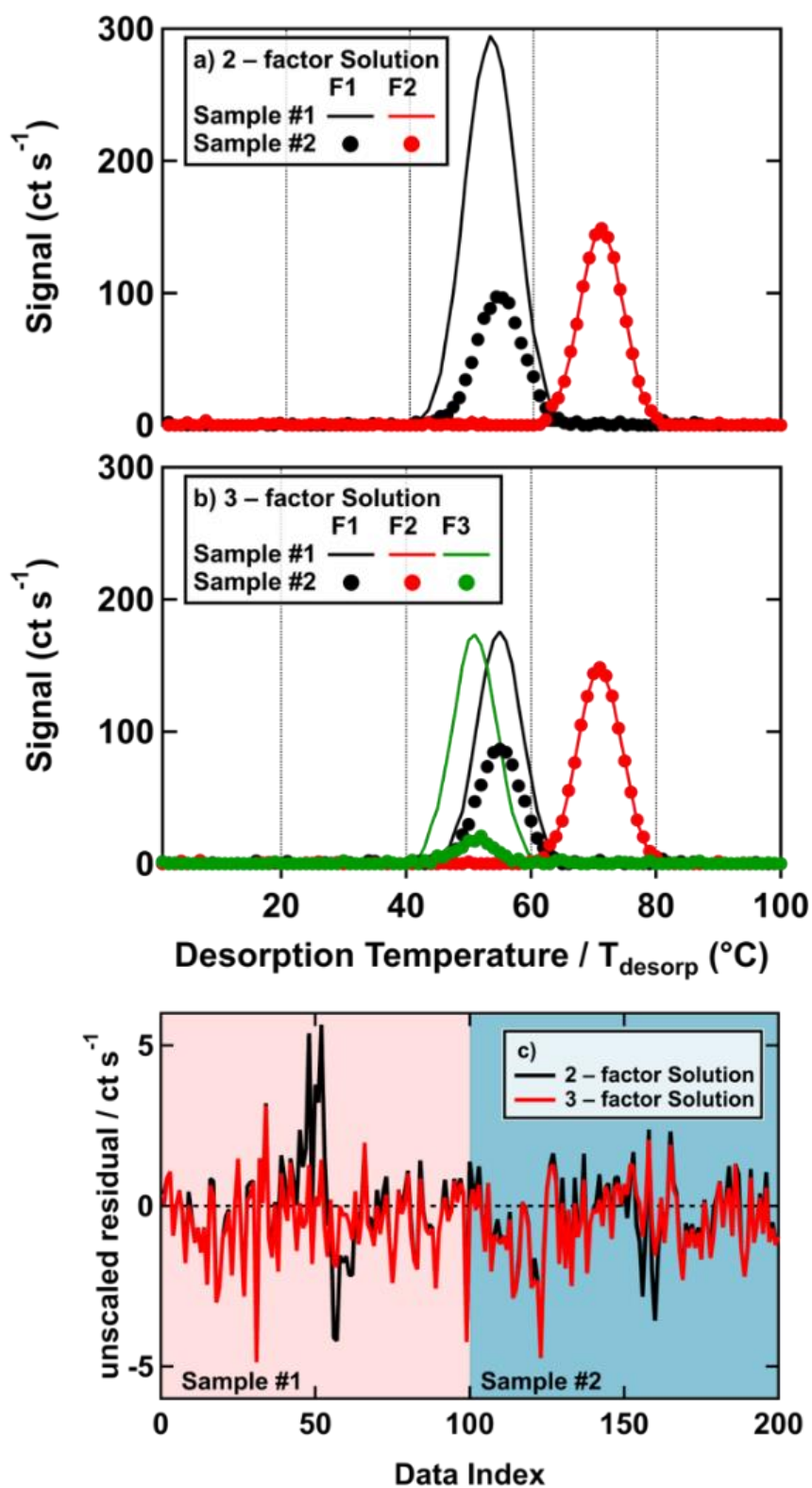


Figure S7. Ion thermograms in the artificial data set.



335

Figure S8. PMF results for the artificial data. Factor thermograms (a and b) and residual as time series (c).

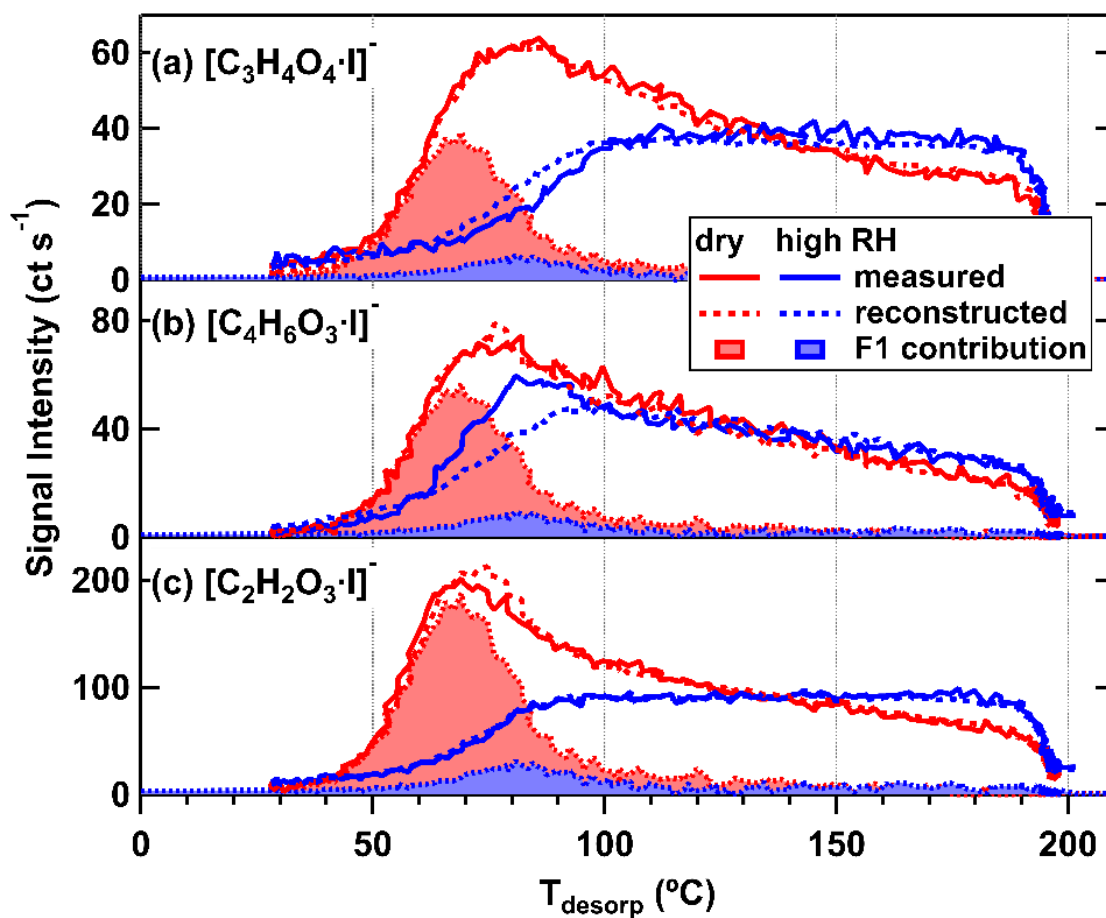


Figure S9. Measured (solid lines) and PMF-reconstructed (dashed) ion thermograms. The colored areas indicate the fraction of the signal that is explained by AF1.

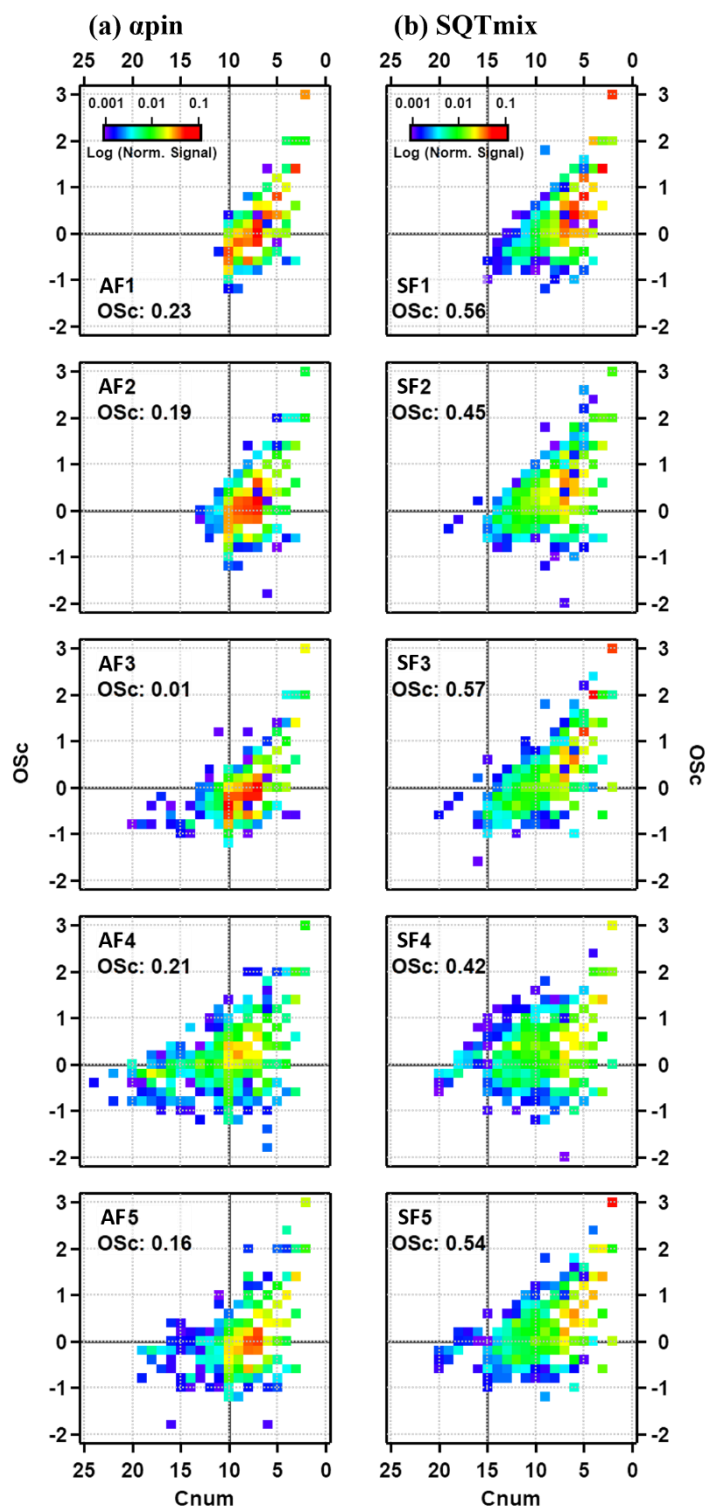


Figure S10. Kroll diagrams for main sample factors in α -pinene(a) and SQTmix (b) SOA particles. For a set of organic compounds containing the same number of carbon atoms, they are grouped into cells with intervals of 0.2 in carbon oxidation state (Osc). Each cell is color-coded by the logarithm of the total sum of normalized signals. While solid horizontal lines mark the Osc values of 0, solid vertical ones indicate the carbon numbers (Cnum) of the respective SOA precursors.

345

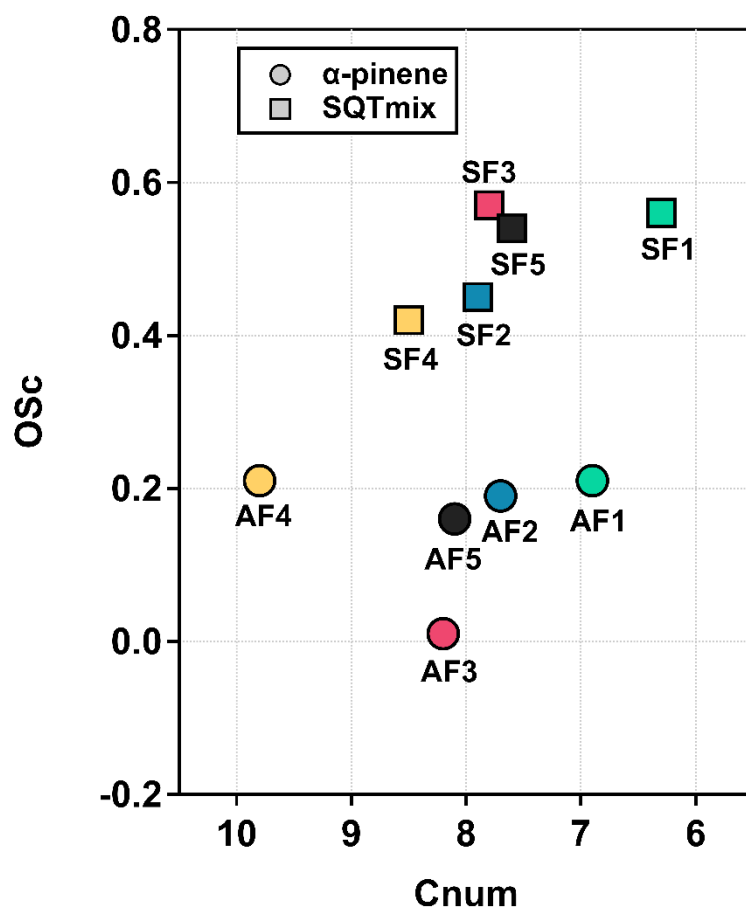


Figure S11. Kroll diagrams for the average carbon oxidation state (OSc) and carbon number of each sample factor in α -pinene (circle) and SQTmix (square) SOA particles.